AD NUMBER

ADB233883

NEW LIMITATION CHANGE

TO

Approved for public release, distribution unlimited

FROM

Distribution authorized to U.S. Gov't. agencies only; Proprietary Information; Oct 97. Other requests shall be referred to US Army Medical Research and Materiel Command, 504 Scott St., Fort Detrick, MD 21702-5012.

AUTHORITY

USAMRMC ltr, dtd 21 Feb 2003

AD_____

GRANT NUMBER DAMD17-96-1-6131

TITLE: Vascular Functional Imaging and Physiological Environment
of Hyperplasia, Non-Metastatic and Metastatic Breast Cancer

PRINCIPAL INVESTIGATOR: Zaver M. Bhujwalla, Ph.D.

CONTRACTING ORGANIZATION: The Johns Hopkins University
                           Baltimore, Maryland 21205-5014

REPORT DATE: October 1997

TYPE OF REPORT: Annual   DTIC QUALITY INSPECTED 2

PREPARED FOR: Commander
               U.S. Army Medical Research and Materiel Command
               Fort Detrick, Maryland 21702-5012

DISTRIBUTION STATEMENT: Distribution authorized to U.S. Government
agencies only (proprietary information, Oct 97). Other requests
for this document shall be referred to U.S. Army Medical Research
and Materiel Command, 504 Scott Street, Fort Detrick, Maryland
21702-5012.

The views, opinions and/or findings contained in this report are
those of the author(s) and should not be construed as an official
Department of the Army position, policy or decision unless so
designated by other documentation.

19980317 152

REPORT DOCUMENTATION PAGE		Form Approved OMB No. 0704-0188

1. AGENCY USE ONLY (Leave blank)	2. REPORT DATE October 1997	3. REPORT TYPE AND DATES COVERED Annual (1 Oct 96 - 30 Sep 97)

4. TITLE AND SUBTITLE
Vascular Functional Imaging and Physiological Environment of Hyperplasia, Non-Metastatic and Metastatic Breast Cancer

5. FUNDING NUMBERS
DAMD17-96-1-6131

6. AUTHOR(S)
Zaver M. Bhujwalla, Ph.D.

7. PERFORMING ORGANIZATION NAME(S) AND ADDRESS(ES)
The Johns Hopkins University
Baltimore, MD 21205-5014

8. PERFORMING ORGANIZATION REPORT NUMBER

9. SPONSORING/MONITORING AGENCY NAME(S) AND ADDRESS(ES)
Commander
U.S. Army Medical Research and Materiel Command
Fort Detrick, Frederick, Maryland 21702-5012

10. SPONSORING/MONITORING AGENCY REPORT NUMBER

11. SUPPLEMENTARY NOTES

12a. DISTRIBUTION / AVAILABILITY STATEMENT

Distribution authorized to U.S. Government agencies only (proprietary information, Oct 97). Other requests for this document shall be referred to U.S. Army Medical Research and Materiel Command, 504 Scott Street, Fort Detrick, Maryland 21702-5012.

12b. DISTRIBUTION CODE

13. ABSTRACT (Maximum 200

Our research proposal consists of the following three closely related aims directed towards understanding the role of vascular, physiological and metabolic properties in the metastatic dissemination of breast cancer. Aim 1: To investigate the relationship between metastatic phenotype and the development of vascularization and evaluate the functionality of the developing vascularization in terms of vascular volume, vascular permeability and relative perfusion. Aim 2: To investigate the effect of increasing (a) tumor vascularization and (b) tumor vascularization and permeability on the formation of metastases. Aim 3: To determine the relationship between metastatic phenotype and intra- and extracellular pH and lactate production. In year 1 we have made substantial progress for the studies outlined for Aim 1 and Aim 3. We have observed a metastatic line to induce a significantly higher vascular volume than a nonmetastatic line. We have also extended our technical capability to noninvasively obtain 3-dimensional maps of vascular volume and permeability. We have found significant differences in the phospholipid metabolism and pH of clones of a highly metastatic human breast cancer line transfected with the metastasis suppressor gene nm23. These results provide further understanding of, and may be exploited to prevent, breast cancer metastasis.

14. SUBJECT TERMS Breast Cancer

15. NUMBER OF PAGES
27

16. PRICE CODE

17. SECURITY CLASSIFICATION OF REPORT	18. SECURITY CLASSIFICATION OF THIS PAGE	19. SECURITY CLASSIFICATION OF ABSTRACT	20. LIMITATION OF ABSTRACT
Unclassified	Unclassified	Unclassified	Limited

Opinions, interpretations, conclusions and recommendations are those of the author and are not necessarily endorsed by the U.S. Army.

_____ Where copyrighted material is quoted, permission has been obtained to use such material.

_____ Where material from documents designated for limited distribution is quoted, permission has been obtained to use the material.

_____ Citations of commercial organizations and trade names in this report do not constitute an official Department of Army endorsement or approval of the products or services of these organizations.

_X___ In conducting research using animals, the investigator(s) adhered to the "Guide for the Care and Use of Laboratory Animals," prepared by the Committee on Care and Use of Laboratory Animals of the Institute of Laboratory Resources, National Research Council (NIH Publication No. 86-23, Revised 1985).

__𝜲__ For the protection of human subjects, the investigator(s) adhered to policies of applicable Federal Law 45 CFR 46.

_____ In conducting research utilizing recombinant DNA technology, the investigator(s) adhered to current guidelines promulgated by the National Institutes of Health.

_____ In the conduct of research utilizing recombinant DNA, the investigator(s) adhered to the NIH Guidelines for Research Involving Recombinant DNA Molecules.

_____ In the conduct of research involving hazardous organisms, the investigator(s) adhered to the CDC-NIH Guide for Biosafety in Microbiological and Biomedical Laboratories.

_____
PI - Signature   Date

Oct. 17, 1997

3

TABLE OF CONTENTS

GENERAL INTRODUCTION TO THE OVERALL RESEARCH PROPOSAL

Vascularization plays a key role in the growth and metastasis of solid tumors [1-6]. In two recent clinical studies, breast cancer patients whose tumors had a high vascular density subsequently went on to develop metastases over a follow up period of 2.5 years [7, 8]. Statistical analyses of these patients showed that vascular density was the single most important factor ($p<0.006$) associated with subsequent formation of metastasis [8]; the other factors examined were epidermal growth factor receptor status ($p<0.01$), node status ($p<0.02$), estrogen receptor status ($p< 0.05$), tumor size ($p<0.06$), tumor grade ($p<0.5$), c-erb-2 expression ($p<0.7$), p53 ($p<0.8$) and tumor type ($p<0.8$). Studies correlating vascularization with metastasis have so far been performed with histological evaluation of excised tissue specimens [7, 8] as a result of which information regarding functioning of vessels is lost. Similarly, the physiological environment of these tumors, in terms of acidity and lactate production remains unknown. Thus a lack of noninvasive methods has left some vital questions about the precise nature of the relationship between vascularization and metastasis unanswered.

Tumor neovascularization is induced by the secretion of angiogenic factors which act as chemotactic factors and mitogens for endothelial cells [1, 4-6]. One of the most potent of these is vascular endothelial growth factor (VEGF). VEGF also increases vascular permeability which in turn may allow cancer cells greater access to the vasculature [9]. In glioblastoma multiformae areas of necrosis and hypoxia show a higher expression of VEGF [10, 11]. Poorly functioning vessels and the associated hypoxia and necrosis may play a role in attracting further vascularization. Areas of hypoxia are also associated with accumulation of lactate and low pH. These two physiological factors attract neovascularization by stimulating the secretion of angiogenic factors from macrophages [12-15]. The secretion of enzymes which degrade the basement membrane in the metastatic process increases at low pH [16, 17]. Thus, vascularization, the physiological environment, and formation of metastases are highly interdependent. An understanding of the role of the physiological environment in vascularization and metastasis, and the dependence of this environment on metastatic phenotype are essential to delineate the relationship between vascularization and metastasis.

Questions which are central to understanding this relationship are - (1) does the metastatic phenotype induce a higher degree of vascularization and is this mediated by modulation of the physiological environment ? (addressed in Specific Aims 1 and 3) (2) If so, do nonmetastatic tumors and preneoplastic tissue exhibit proportionately lower vascularization ? (addressed in Specific Aims 1 and 2) (3) Which particular property of the vascularization e.g. permeability, volume or relative perfusion is the dominant factor in the dependence of metastasis on vascularization ? (addressed in Specific Aims 1 and 2) (4) Is a significant fraction of the vessels observed in the histological studies non-functional and does the resultant unsuitable environment induce expression of signals or substances which prompt and enable the cells to metastasize ? (addressed in Specific Aim 1). The overall goal of this research proposal is to use noninvasive Magnetic Resonance (MR) Imaging (I) and Spectroscopy (S) to answer the questions posed above.

The research proposed consists of three closely related aims designed to unravel the complex relationship between vascularization and metastasis. Our overall goal in this project is to determine key vascular and physiological properties which result in the close relationship between vascular density and metastasis as this information may ultimately be used to prevent tumor metastasis. We had proposed the following three aims:

Aim 1: To investigate the relationship between metastatic phenotype and the development of vascularization and evaluate the functionality of the developing vascularization in terms of vascular volume, vascular permeability and relative perfusion.

5

<u>Hypothesis #1</u>: More metastatic lines will exhibit a higher level of vascularization and permeability for similar volumes. A significant number of vessels detected by immunoperoxidase staining will not be functional and this number will increase with the size of the tumor.

<u>Aim 2</u>: To investigate the effect of increasing (a) tumor vascularization and (b) tumor vascularization and permeability on the formation of metastases.
<u>Hypothesis #2:</u> Higher vascularization and permeability will lead to an increase or an earlier incidence of metastases for all the lines.
(Aims 1 and 2 are related to questions 1-4 outlined in background)

<u>Aim 3:</u> To determine the relationship between metastatic phenotype and intra- and extracellular pH and lactate production.
<u>Hypothesis #3</u>: More metastatic lines will be more glycolytically active *in vivo*, creating an environment of high lactate and low extracellular pH for volume matched lesions.
(Aim 3 is related to question 1 outlined in background)

We have made significant progress in performing studies proposed in Aim 1 and Aim 3.

PROGRESS MADE IN AIM 1 (TWO STUDIES)

<u>Aim 1</u>: To investigate the relationship between metastatic phenotype and the development of vascularization and evaluate the functionality of the developing vascularization in terms of vascular volume, vascular permeability and relative perfusion.

AIM 1 - STUDY 1

Quantitative Magnetic Resonance Imaging of Vascular Volume and Permeability

James F. Glockner, Dmitri Artemov and Zaver M. Bhujwalla

ABSTRACT

We used the distribution of the intravascular paramagnetic contrast agent albumin-GdDTPA (gadolinium diethylenetriamine pentaaceticacid) to quantitatively image vascular volume and permeability of highly metastatic human MDA-MB-231 breast tumors grown in the mammary fat pad (mfp) and flank of SCID mice, and lowly metastatic RIF-1 tumors grown in the flank of C3H mice. The studies were performed to understand the role of vascular properties in the dissemination of solid tumors. Quantitative images were obtained with an in-plane resolution of 125 μm and slice thickness of 700 μm. Tumor volumes ranged from 100-300 mm^3. Vascular volumes in μl/gm of MDA-MB-231 mammary fat pad and flank tumors were significantly higher than for size matched RIF-1 tumors. Vasculature of MDA-MB-231 flank tumors was the most permeable. Both vascular volume and permeability values were spatially heterogeneous for both tumor types. In the images, regions with high vascular volume did not coincide spatially with regions of high permeability. Studies relating vascular volume to metastatic potential merit further investigation and may indicate a possible role for MRI in the prediction of metastatic potential.

MATERIALS AND METHODS

For our experiments we used a highly metastatic human breast cancer line (MDA-MB-231) [18] and a lowly metastatic C3H mouse fibrosarcoma (RIF-1) line [19]. The metastatic human breast cancer cell line was grown in the orthotopic site of the mammary fat pad (mfp) or the flank (f) of mice, since the cell line metastasizes to a significantly lesser extent when grown in a heterotopic site like the flank [20]. MDA-MB-231 cells were inoculated in the right flank and the right upper thoracic mammary fat pad (mfp) of severe combined immune deficient (SCID) mice in a volume of 0.05ml Hanks balanced salt solution, at a concentration of 10^6 cells/0.05ml. RIF-1 tumor cells, at a concentration of 10^5 cells/0.05ml, were inoculated in a volume of 0.05ml Hanks balanced salt solution in the right flank of female C3H mice.

Tumors were examined at volumes of 100-300 mm^3. Tumor volumes were calculated from caliper measurements of tumor axes (a,b,c) using the equation for an elliptical volume ($\pi/6$)abc. Imaging studies were performed on a GE CSI 4.7T instrument equipped with shielded gradients. Alb-GdDTPA was synthesized in our laboratory according to the procedure originally described by Ogan *et al.*, [21]. Images were obtained with a solenoid coil wrapped around the tumor. A small capillary filled with water doped with GdDTPA was attached to the side of the coil to (a) serve as an intensity reference, (b) ensure that spatial registration was identical for all images, and (c) reference histological sections with images. Animals were anesthetized with a mixture of ketamine and acepromazine (50 mg/kg, 5 mg/kg). The tail vein of the animal was catheterized before it was

placed in the magnet. Animal body temperature was maintained at 37°C by heat generated from warm water circulating through a pad. Studies were carried out on MDA-MB-231 tumors (n=6 for mfp tumors; n=4 for flank tumors) and RIF-1 tumors (n=4).

For the imaging studies, T_1 maps (using saturation recovery) were obtained with three recovery time intervals (100ms, 500ms, 1s) for a 0.7 mm sagittal slice through the center of the tumor (Field of View =16mm; 128x128 matrix; number of averages =2; sw=20000; in-plane resolution = 125 μm; repetition time =100ms; echo time =16ms). A 0.2ml bolus of a solution of 60mg/ml alb-GdDTPA made up in saline was injected through the tail vein (dose of 500mg/kg). T_1 maps were obtained before and at 3 time intervals of 20 minutes each after the intra-venous (i.v.) injection. Data acquisition for the first post contrast agent map was initiated 10 minutes after the i.v. injection to allow for equilibration of the contrast agent. At the end of the imaging studies, the animal was sacrificed, 0.5 ml of blood was withdrawn from the inferior vena cava, and the tumors were excised and fixed in 10% buffered formalin for sectioning and staining.

Vascular volume and permeability product surface area (PS) maps were generated from the ratio of $\Delta(1/T_1)$ values in the images to that of blood using an IDL (Interactive Data Language, Research Systems, Inc.) program. The slope of $\Delta(1/T_1)$ ratios versus time in each pixel was used to compute (PS) while the intercept of the line at zero time was used to compute vascular volume [22, 23]. Thus, vascular volumes were corrected for permeability of the vessels within each pixel.

Five 5μm thick paraffin embedded histological sections were obtained from the imaged slice and immunohistochemically stained for VEGF expression. A rabbit polyclonal anti-VEGF antibody (Santa Cruz Biotechnology, Santa Cruz, CA) cross reactive with mouse, rat and human tissue was used at a 1:200 dilution factor [24] . Negative controls were obtained using all reagents except the primary antibody. Adjacent sections were stained with haematoxylin and eosin for morphological information.

RESULTS

Both vascular volume and permeability were spatially heterogeneous for both tumor types. Most tumors showed a higher vascular volume around the periphery which was consistent with the presence of higher vessel density in the histological sections. Regions with high vascular volume did not coincide entirely with regions of high permeability but there was some overlap. Figures 1a, b, c and d are high-resolution saturation recovery spin-echo images (recovery time of 1s which provides strong T1 contrast) showing the uptake and distribution of alb-GdDTPA in a mfp MDA-MB-231 tumor (vol. 250 mm^3) before and at median time points of 20, 40 and 60 min after injection. The corresponding vascular volume and permeability images are shown in Figures 2a and b; these images are contrast enhanced for clarity. Figures 3a, b, c and d are high-resolution saturation recovery spin-echo images (recovery time of 1s) showing the uptake and distribution of alb-GdDTPA in a MDA-MB-231 tumor inoculated in the flank (volume 187 mm^3). The images were obtained before and at median time points of 20, 40 and 60 min after injection of alb-GdDTPA. The corresponding vascular volume and permeability images are shown in Figures 4a and b; these images are contrast enhanced for clarity. This tumor demonstrated the highest permeability in the entire study and also contained a fairly large focus of necrosis.

Table 1 contains mean vascular volume and permeability values calculated by averaging over the entire imaged slice of each tumor for the three combinations of tumor type and inoculation site. When compared to RIF-1 tumors (vascular volume 18.7 ± 4 μl/gm), MDA-MB-231 mfp tumors showed the highest vascular volume (46.6 ± 9 μl/gm) followed by MDA-MB-231 flank tumors (37.4 ± 8.5 μl/gm). MDA-MB-231 flank tumor vasculature was the most permeable and also showed a high expression of VEGF in terms of staining density.

VEGF staining was most intense around necrotic areas. A coarse spatial agreement was observed between areas with high VEGF expression in the histological section and areas of high permeability observed in the MRI images for the MDA-MB-231 line. We are unable to comment on the expression of VEGF in RIF-1 tumors because of the cross reactivity of the VEGF antibody.

The volume doubling time of RIF-1 tumors in our laboratory was approximately 72 h, which is consistent with the doubling time for this tumor model reported in other studies [19] . RIF-1 tumors were palpable (~ 1-2 mm diameter) within 12 days of inoculation. MDA-MB-231 tumors exhibited a significantly longer latent period than RIF-1 tumors and were palpable only after 4-6 weeks of inoculation. The volume doubling time of MDA-MB-231 tumors was approximately 14 days which is consistent with values reported by Zhang et al.[18]. Metastatic nodules (3 mm diameter) were observed in the left and right axillary lymph node regions when mfp tumors were excised at volumes of 900 mm3. Histological sections of excised liver, when examined, also showed metastatic foci.

Figure 1

(a) (b) (c) (d)
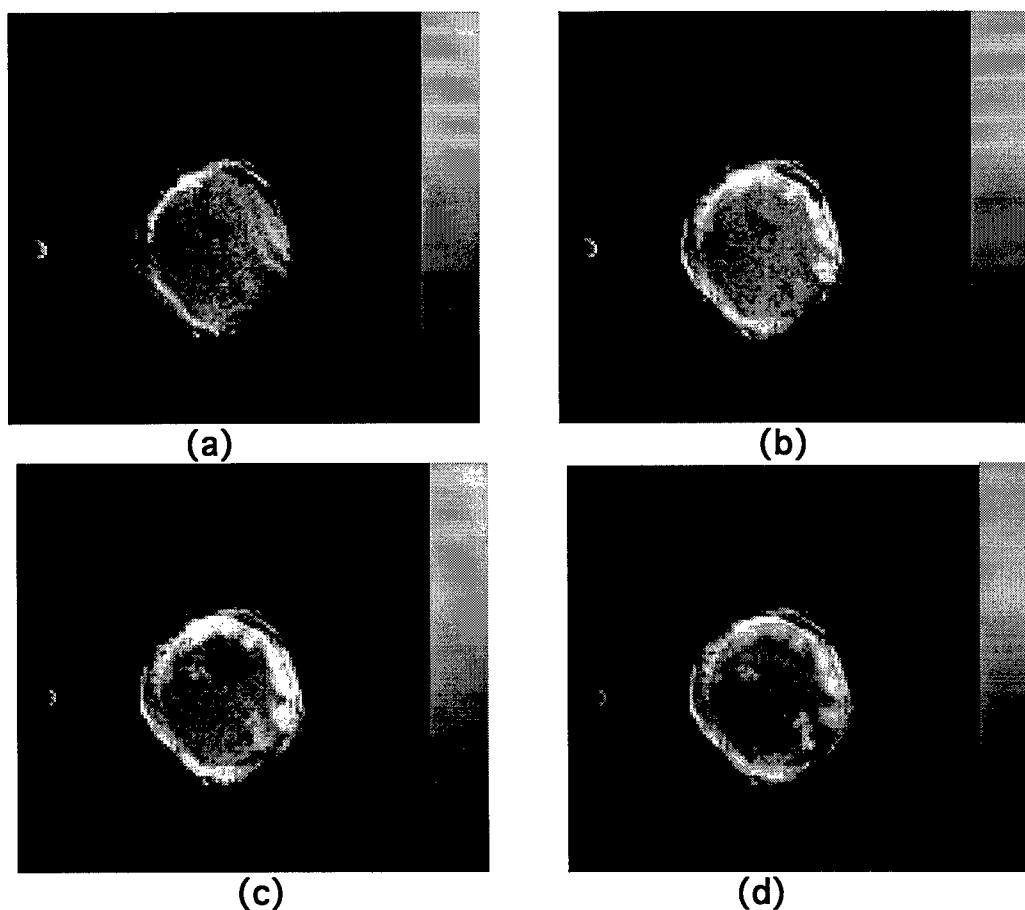
Figure 1: High-resolution saturation recovery spin-echo images (recovery time of 1s) showing the uptake and distribution of alb-GdDTPA in a mfp MDA-MB-231 tumor (volume 250 mm3) (a) before and at (b) 20, (c) 40 and (d) 60 min after injection of alb-GdDTPA. The small glass capillary containing water doped with GdDTPA can also be observed in the images. Details of image acquisition parameters are described in the Methods section.

Figure 2

1000 µl/gm

(a)

50µl/gm-min

(b)
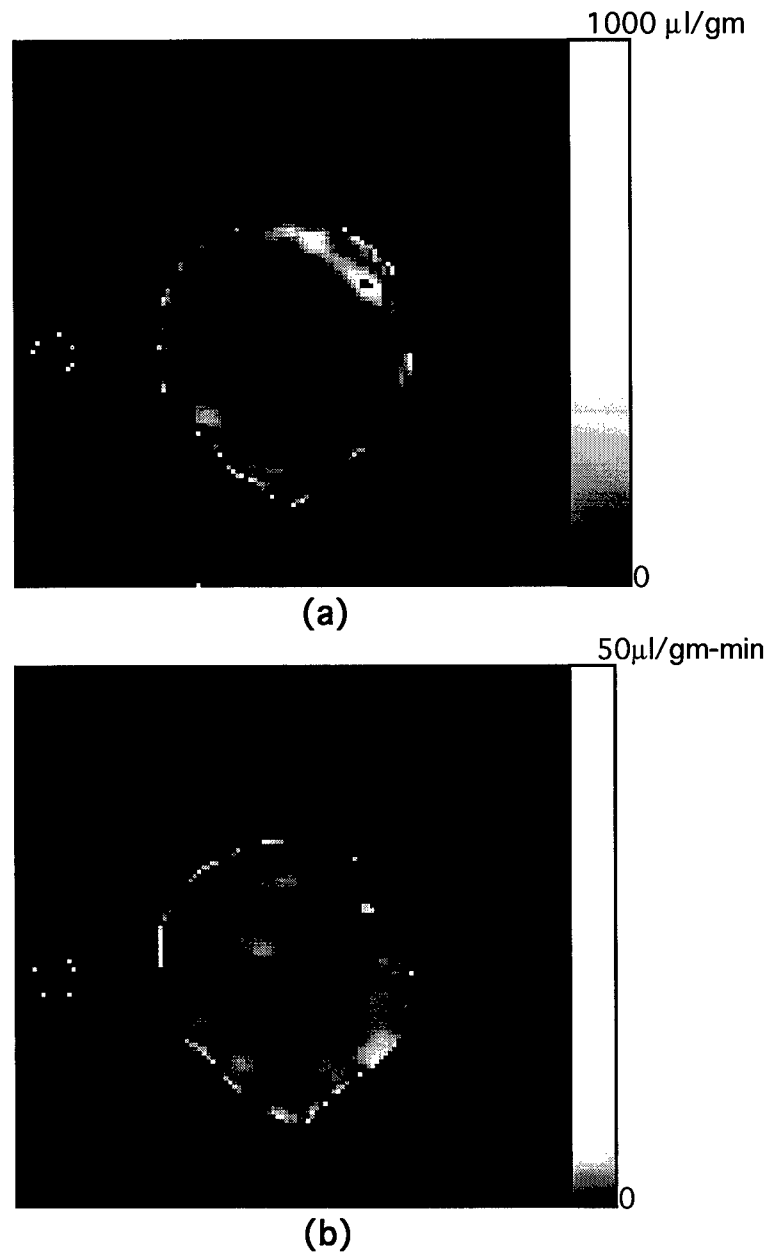
Figure 2: (a) Vascular volume and (b) permeability images obtained for tumor shown in Figure 1; these images are contrast enhanced for clarity.
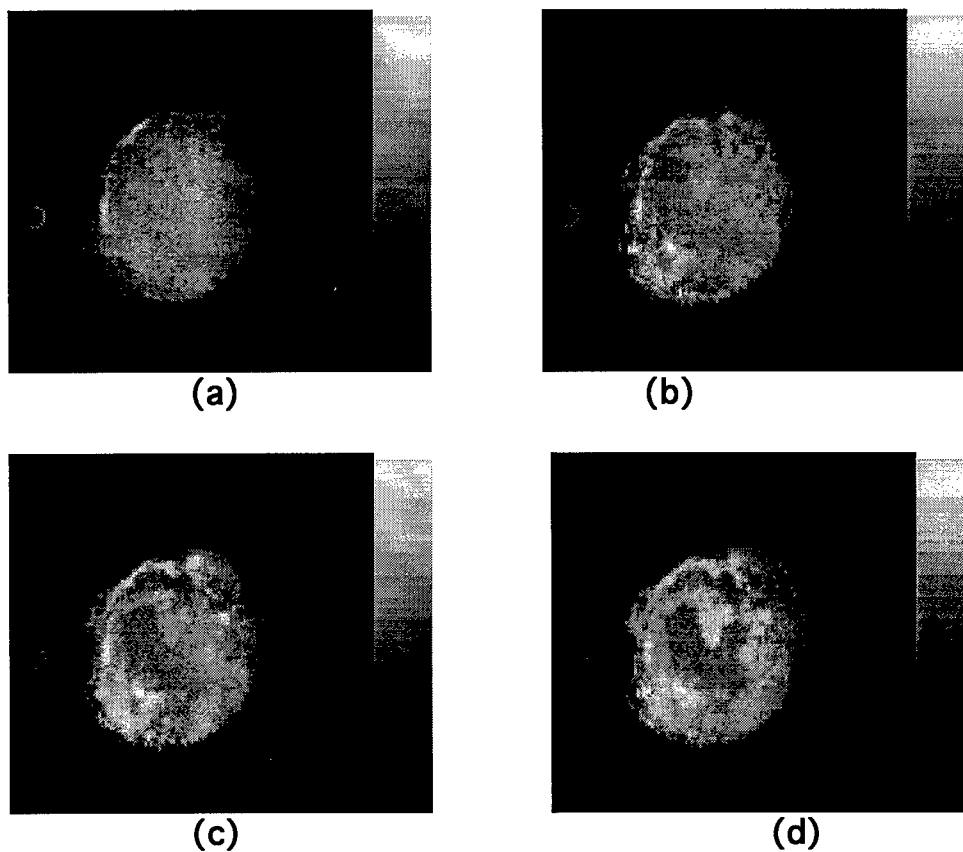
Figure 3

Figure 3: High-resolution saturation recovery spin-echo images (recovery time of 1s) showing the uptake and distribution of alb-GdDTPA in a flank MDA-MB-231 tumor (volume 187 mm3) (a) before and at (b) 20, (c) 40 and (d) 60 min after injection of alb-GdDTPA. The small glass capillary containing water doped with GdDTPA can also be observed in the images. Details of image acquisition parameters are described in the Methods section.
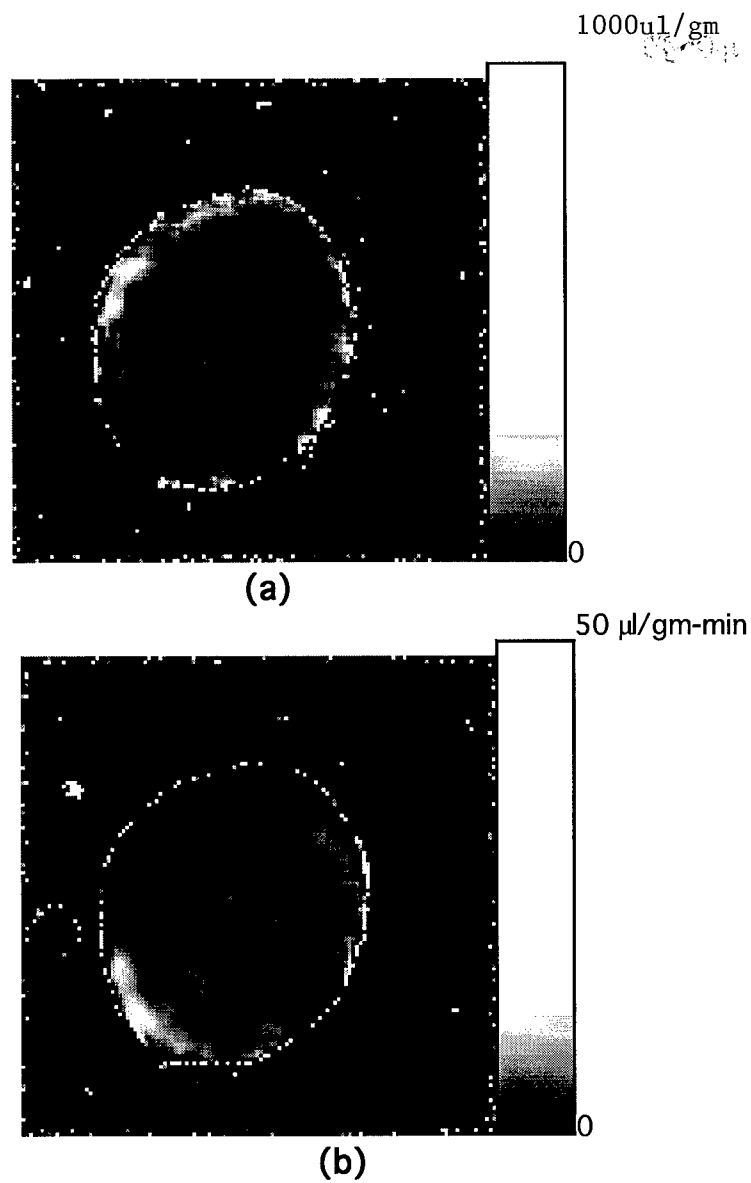
Figure 4

1000ul/gm

(a)

50 µl/gm-min

(b)

Figure 4: (a) Vascular volume and (b) permeability images obtained for tumor shown in Figure 3; these images are contrast enhanced for clarity.

Table 1.

Mean vascular volume and permeability values calculated by averaging over the entire imaged slice of each tumor for the three combinations of tumor type and inoculation site.

Tumor type	Vascular volume (μl/gm)	Permeability (μl/gm-min)
MDA-MB-231 (mfp); n=6	46.6 ± 9* (p<0.05, compared to RIF-1)	0.85 ± 0.13
MDA-MB-231 (f); n=4	37.4 ± 8.5* (p<0.09, compared to RIF-1)	1.64 ± 0.26* (p<0.02 compared to mfp; p<0.08 to RIF)
RIF-1 (f); n=4	18.7 ± 4	0.92 ± 0.23

Values represent Mean ± 1 S.E.M (p values for 2-tail unpaired t-test); flank (f); mammary fat pad (mfp). * indicates significance.

DISCUSSION AND CONCLUSIONS

Values of vascular volume and permeability were heterogeneous. When averaged over the entire imaged slice, values of vascular volume and permeability were in good agreement with those obtained previously using radioactively labeled albumin (M.W.60,00) for the RIF-1 tumor model [22, 23]. There are no literature values of vascular volume and permeability available for comparison for the MDA-MB-231 tumors but the values fall within the ranges observed using radioactively labeled albumin for other tumor models [25]. MRI measurements of vascular volume were obtained by assuming fast exchange of water protons between vascular, interstitial and cellular compartments in the tumors. While tissue vascular volumes obtained based on this assumption have a high correlation with conventional radioisotope measurements [26] intermediate exchange has been detected in isolated perfused hearts [27]. The assumption of fast exchange may therefore lead to a systematic error not exceeding 15% in the estimate of vascular volume[28] .

Vascular volume was consistently higher around the periphery of the tumors consistent with previous observations that peripheral vascularization was one of two basic patterns of tumor vascularization, the other being central vascularizatin [29]. Tumor-induced blood vessels are fragile and highly permeable. Tumor cells may contribute to vascular permeability by expressing vascular permeability factors such as VEGF. Dvorak et al [30] observed that the permeability of vessels within a given tumor was not uniform, but varied extensively. Vessels at the periphery had the highest permeability, whereas vessels at the core were the least permeable. In our study, there was some evidence of higher vascular permeability at the periphery of most of the tumors. However, since it was possible to overlay vascular volume and permeability maps we also determined that the spatial distributions of vascular volume and permeability did not coincide entirely. In fact there were some regions with very high permeability which, in fact, had very low vascular volumes. One possible explanation for these observations is that areas with low vascular

volume may also contain the most leaky and non-functional vasculature. Spatially, the distribution of VEGF coincided with areas of high permeability. Recently, Demsar *et al.* [31] have also observed that regions of high vascular volume do not necessarily coincide with regions of higher permeability .

The MDA-MB-231 cell line was originally isolated from the pleural effusions of a patient with breast carcinoma. The line is highly metastatic when inoculated in the mammary fat pad but rarely metastasizes when inoculated in the flank [18]. The RIF-1 (radiation-induced fibrosarcoma) tumor line arose in the hind limb of a C3H/Km mouse which received fractionated irradiation over 12 weeks. A flank tumor burden in excess of even 10 g does not metastasize [19, 32]. Although it is an animal tumor model, its nonmetastatic behavior in the flank coupled with the fact that independent vascular volume and permeability measurement were available for RIF-1 flank tumors for comparison with our MRI technique made it an attractive choice. It is interesting to note that despite the dramatic difference in volume doubling time between the RIF-1 and MDA-MB-231 model (3 days vs 14 days), the vascular volume of MDA-MB-231 tumors was significantly higher than for the RIF-1 tumors. Yet, RIF-1 tumors at the volumes studied here, do not exhibit necrosis. The balance between tumor growth, vascular volume, and necrosis is complex and will rest in part upon the cell cycle time, the cell loss factor, the rate of dead cell clearance, the ability of cells to generate an angiogenic response, the endothelial cell proliferation rate, the growth fraction and the energy requirements of cells [33, 34].

The vasculature of the MDA-MB-231 line was significantly more permeable in the heterotopic site. compared to the orthotopic site. Since flank tumors metastasize to a lesser extent than fat pad tumors the results obtained suggest that vascular permeability (as measured by alb-GdDTPA) alone may not play a significant role in metastasis.

It is possible to detect significant differences in vascular volume and permeability using MRI and, within the constraints of our present study we observed that the lowly metastatic RIF-1 tumor generated significantly lower vascular volume than the highly metastatic MDA-MB-231 tumor. The relationship between vascular volume and metastatic potential merits further investigation with MRI for tumors with different embryologic origins and different histologies, with differing metastatic behavior. If such a relationship is demonstrated for a wide range of tumors, a clinical MRI method for determining vascular volume will play a significant role in the prediction of metastatic potential.

Proprietary data

3-Dimensional MRI Quantitation of Tumor Vascular Volume and Permeability

Dmitri Artemov and Zaver M. Bhujwalla

INTRODUCTION

To further understand the role of vascularization and permeability in tumor metastasis it is necessary to relate these parameters to the expression of VEGF (2-3), to histomorphological information such as necrosis and to immunohistochemical staining of growth factors and protein expression (4). One of the perennial problems in relating noninvasive images to hispathological information is accurate spatial co-registration. This problem of spatial co-registration can be simplified by obtaining 3-dimensional (3-D) reconstructed maps of the parameter being quantitated by MRI to compare with 3-D reconstructed histopathological maps. 3-D reconstructed quantitative maps also provide more comprehensive information, compared to single slice images, of the parameter being measured. Here we present results of 3-D mapping of tumor vascular volume and permeability. The images were reconstructed from multi-slice distribution of the intravascular paramagnetic contrast agent albumin-GdDTPA (gadolinium diethylenetriamine pentaacetic acid), obtained from multi-slice T_1 maps. 3-D maps were obtained for a metastatic human breast cancer cell line (MDA-MB-231) and a non metastatic human breast cancer line (MCF-7), grown in the flank of severe combined immune deficient (SCID) mice.

METHODS AND MATERIALS

Imaging studies were performed on a GE Omega 4.7T instrument using a solenoidal coil wrapped around the tumor (volumes 100-300mm^3). The tail vein of the anaesthetized animal was catheterized before it was placed in the magnet. Animal body temperature was maintained at 37oC by heat generated from a warm water pad. 3-D distributions of relaxation rates (T_1^{-1}) in tumors were obtained by a saturation recovery method combined with fast 3-D T_1 SNAPSHOT-FLASH imaging (5) (flip angle of 7°, echo time of 2ms). Images of 8 slices (slice thickness of 1mm) acquired with an in-plane spatial resolution of 250mm (64x64 matrix, 16mm field of view, NS=16) were obtained for 3 relaxation delays (100ms, 500ms, and 1s) for each of the slices. Thus, 64x64x8 3-D T_1 maps were acquired within 7 minutes. Images were obtained before i.v. administration of 0.2ml of 60 mg/ml albumin-GdDTPA in saline (dose of 500mg/kg) and repeated every 8 minutes, starting 10 minutes after the injection, up to 32 minutes. An M_O map with a recovery delay of 7s was acquired once at the beginning of the experiment. 3D relaxation maps were reconstructed from data sets for three different relaxation times and the M_O data set. At the end of the imaging studies, the animal was sacrificed, 0.5 ml of blood was withdrawn from the inferior vena cava, and tumors were excised and fixed in 10% formalin for sectioning and staining. Vascular volume [VV] and permeability product surface area (PS) maps were generated from the ratio of $\Delta(1/T1)$ values in the images to that of blood. The slope of $\Delta(1/T1)$ ratios versus time in each pixel was used to compute (PS) while the intercept of the line at zero time was used to compute vascular volume (1). Thus, vascular volumes were corrected for permeability of the vessels. IDL software was used for data analysis.
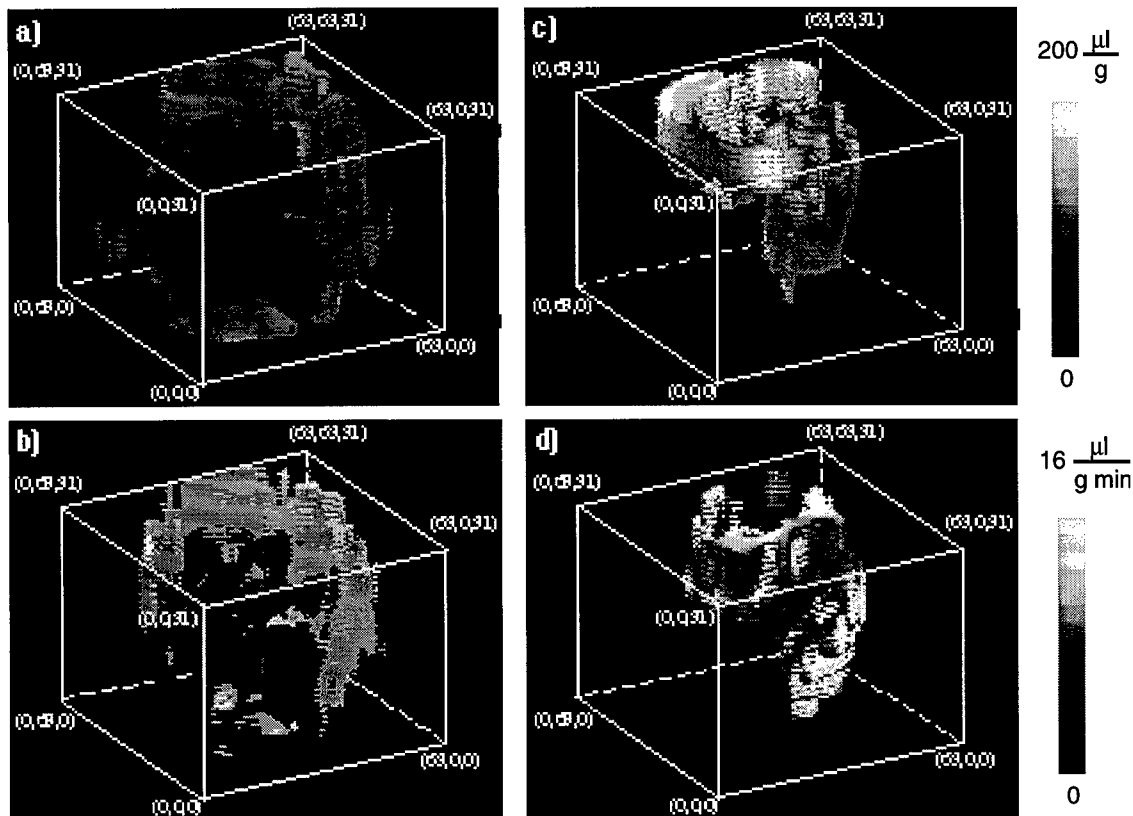
RESULTS

Figure 1 a, b, c and d show vascular volume and permeability images for MCF-7 (a,b) and MDA-MB-231 tumors (c,d). The 3-D views were composed with the Slicer routine of the IDL program after zero-filling experimental data to 64x64x32 pixels. This matches the geometrical appearance of the images to the field of view of the imaging experiment (16x16x8mm). A wedge is placed through Figure 1a and b to demonstrate the distribution of vascular volume and permeability through the core of the tumor.

Vascular volume and permeability were spatially heterogeneous. As observed before regions with high vascular volume did not coincide spatially with regions of high permeability although there was some overlap. Vascular volume and permeability was more uniform for the smaller MDA-MB-231 tumor. 3-D maps for this small tumor also contain a portion of the chest wall. Representative 2D slices through the center of the tumor for the images presented in Fig.1 are shown in Fig.2
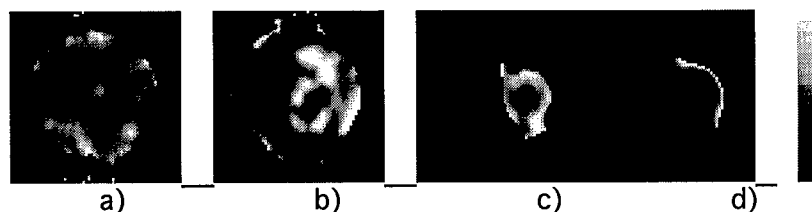
Figure 2 a) MCF-7 VV; b) MCF-7 PS; c) MDA VV; d) MDA PS.
Gray scale values as in Figure 1.

16   Proprietary data

DISCUSSION AND CONCLUSION

We have shown here, for the first time, the feasiblity of obtaining noninvasive quantitative 3-D maps of tumor vascular volume and permeability. The use of saturation recovery rather than inversion recovery significantly reduced the acquitision time of the images. Such technological availability provides a cutting-edge for research aimed at understanding the role of vascularization and permeability in tumor metastasis.

PROGRESS MADE IN AIM 3

<u>Aim 3:</u> To determine the relationship between metastatic phenotype and intra- and extracellular pH and lactate production.

Nm23-transfected MDA-MB-435 human breast carcinoma cells form tumors with altered phospholipid metabolism and pH. A ^{31}P NMR study *In vivo* and *In vitro*

Zaver M. Bhujwalla and Eric O. Aboagye

IN COLLABORATION WITH

Charmaine E. Mendola, Joseph M. Backer
Department of Microbiology and Immunology, New York Medical College, Valhalla, NY 10595

and

Robert J. Gillies
Department of Biochemistry, University of Arizona, Tucson, AZ 85724

ABSTRACT

Nm23 genes are implicated in the control of the metastatic potential of tumor cells. In order to understand the impact of nm23 genes on tumor physiology and metabolism we undertook a ^{31}P NMR study of tumors formed in the mammary fat pad of SCID mice by MDA-MB-435 human breast carcinoma cells transfected with cDNA encoding wild type and catalytically inactive nm23-1 and nm23-2 proteins. Tumors formed by MDA-MB-435 cells transfected with vector alone, and by untransfected MDA-MB-231 cells were used as controls. All transgene tumors exhibited significantly higher levels of phosphodiester (PDE) compounds relative to phosphomonoester (PME) compounds *in vivo* compared to control tumors. High resolution ^{31}P NMR spectra of tumor extracts identified the components of the PDE region as the membrane breakdown products glycerophosphocholine (GPC) and glycerophosphoethanolamine (GPE) while the PME region consisted of the membrane precursors phosphocholine (PC) and phosphoethanolamine (PE). These differences were also observed for spectra obtained from cells growing in tissue culture and may reflect differences in fatty acid requirements or differences in membrane turnover and degradation rates following transfection with nm23. ^{31}P NMR measurements of intra- and extracellular pH revealed significant differences between control and transgene tumors. Intracellular pH was significantly lower for transgene tumors formed by MDA-MB-435 cells transfected with cDNA encoding wild type nm23-1 and nm23-2 proteins while extracellular pH was significantly higher for transgene tumors formed by MDA-MB-435 cells transfected with cDNA encoding wild type nm23-1, nm23-2 and catalytically inactive nm23-2 proteins. The results demonstrate the utility of ^{31}P NMR spectroscopy in establishing the role of nm23 genes in tumor metabolism and metastatic dissemination.

INTRODUCTION

Despite continuing advances in the molecular characteristics of events promoting metastasis, little impact has been made on therapy or survival for patients with advanced metastatic tumors [35]. This is partly due to the lack of identifiable targets against which to design antineoplastic agents to control

Proprietary data

the metastatic spread of cancer. Multinuclear NMR methods have a unique role to play in answering this challenge by providing an understanding of the biochemical and physiological mechanisms involved in invasion and metastasis. Such an understanding can identify rational targets for therapy. Recently it was shown that the nm(nonmetastatic)23 gene is related to suppression of metastasis; the metastasis suppression function of the nm23 gene was proposed on the basis of correlation and transfection studies in murine and human systems [36, 37].

Currently, two highly homologous and evolutionary conserved nm23 genes, nm23-1 and nm23-2, have been identified in mammals [38, 39] and two nm23 genes (nm23-H1 and nm23-H2) have been identified in humans [40, 41]. The two murine nm23 genomic DNAs have been cloned and sequenced [42, 43]. The human nm23-H1 and nm23-H2 genes have been localized to chromosome 17q21[44, 45]. These genes encode 17 kDa proteins which have been identified as nucleoside diphosphate kinases (NDPK) A and B, which form homomers and heteromers. In addition NDPK B displays an increasing list of other activities that are apparently unrelated to its catalytic functions. However, the cellular mechanisms by which the nm23 protein suppresses metastatic phenotypic expression is as yet unknown. Here we have used ^{31}P NMR spectroscopy to study metabolic and physiological characteristics of tumors induced in SCID mice by MDA-MB-435 human breast carcinoma cells transfected with wild type and catalytically inactive cDNA of nm23-1 and nm23-2. Such studies can provide further understanding of the cellular functions of nm23 and of the mechanisms of action of nm23-1 and nm23-2 genes and their role in metastatic dissemination of tumor cells.

MATERIALS AND METHODS

Coding sequences of normal nm23-1 and nm23-2 proteins and catalytically inactive mutant nm23-1T and nm23-2T proteins in which his118 was substituted by tyrosine, were cloned into the eucaryotic expression vector pβalPstNeo under control of a constitutive HCMV promoter ^{4} [45, 46] . NM-23 proteins were rendered catalytically inactive by this substitution, since phospho-his118 is an obligatory phosphorylated intermediate in the NDPK reaction [47]. The vector contains a neo-resistance gene under control of SV40 promoter. MDA-MB-435 breast carcinoma cells were transfected with nm23 constructs using a Lipofectin kit (BRL) and selection of transfected clones was done in the presence 800 μg/ml G418. Nm23 transfected pooled clones of MDA-MB-435 were then transfected with p1Zsp-βgluc (puro), a mammalian expression vector containing bacterial β-glucuronidase under control of a constitutive HCMV promoter and puromycin resistance gene under control of SV-40 promoter (Gift from Dr. T. Jones, Lederle Laboratories). Selection of clones expressing bacterial β-glucuronidase was done in the presence of 0.375 μg/ml puromycin and 800 μg/ml G418. Pooled clones of double transfected cells named MDA-MB-435-V, MDA-MB-453-1β, MDA-MB-435-1Tβ, MDA-MB-435-2β, and MDA-MB-435-2Tβ for vector alone, nm23-1/β-glucuronidase, nm23-1T/β-glucuronidase, nm23-2/β-glucuronidase, and nm23-2T/β-glucuronidase transfections respectively were maintained in the presence of 0.375 μg/ml puromycin and 800 μg/ml G418. Presence of transgenes was confirmed by PCR analysis, Western blot analysis, and staining with 5-bromo-4-chloro-3-indol 1 glucuronide (X-glu).

MDA-MB-435-V, MDA-MB-435-1β, MDA-MB-435-1Tβ, MDA-MB-435-2β, MDA-MB-435-2Tβ and wild type MDA-MB-231 cells (as an additional control) were injected in the upper left thoracic mammary fat pad (mfp) of SCID mice (10^6 cells in 0.05ml of Hank's balanced salt solution). The experimental protocol was approved by the Institutional Animal Care and Use Committee. Mice were anesthetized with ketamine (50mg/kg; Aveco Ltd.) and acepromazine (5mg/kg; Aveco Ltd.). Tumor volumes, were calculated from caliper measurements of tumor axes (a,b,c) using the

Proprietary data

equation for an elliptical volume $(\pi/6)abc$. Tumor volumes were measured just prior to performing the ^{31}P NMR spectroscopic studies. Volumes of tumors used in this study were of the order of 300 mm^3. A separate group of 'large' MDA-MB-435-1Tβ tumors with volumes of 700 mm^3 were also examined.

^{31}P NMR spectroscopic studies were performed on a GE CSI 4.7T instrument equipped with shielded gradients. Spectra were obtained with home-built solenoidal coils fitted around the tumor. Animal body temperature was maintained at 37°C by heat generated from a pad circulating with warm water. For the ^{31}P NMR studies mice were injected intraperitoneally with a solution of the extracellular pH marker 3-APP (3-aminopropylphosphonate; Sigma Ltd.) administered in a volume of 0.2ml saline (480mg/kg) following anesthetization. Fully relaxed ^{31}P NMR spectra were obtained using a 45° flip angle, na=64, pd =5s. Parameters were determined from two spectra obtained per tumor. NMR examinations were completed within 20 minutes. Extracellular pH (pHe) was obtained from the chemical shift of 3-APP [48] and intracellular pH from the chemical shift of Pi [49] from the endogenous reference α-NTP set to -7.57 ppm. pHe was calculated from the relationship pH = 6.91 + log[$\delta_{3\text{-APP}}$ - 21.11]/(24.3 - $\delta_{3\text{-APP}}$). pHi was calculated from the relationship pH = 6.66 + log[δ_{Pi} - 0.65]/(3.11 - δ_{Pi}). Data sets were processed using an exponential line broadening factor of 22 Hz. A non-linear least squares curve fitting routine, using an in-house computer program for MR data analysis written by Dr. D. C. Shungu, was used to determine peak areas in the time domain.

Statistical analysis of the data was performed using StatView II version 1.04, 1991 (Abacus Concepts, Inc., Berkeley, CA, USA). One factorial analysis of variance (ANOVA) together with a 2-tailed unpaired Student's t-test was used to evaluate the statistical significance of the data.

RESULTS

All the cell lines were tumorigenic in SCID mice. Growth rates for control and transgene tumors were similar, with a volume doubling time of 12-14 days. The most striking difference between ^{31}P NMR spectra of control (Figure 1) and transgene tumors (Figure 2) was a marked increase of the peak in the PDE region relative to the PME region in spectra of transgene tumors. Elevation of this peak, comprising of membrane phospholipid breakdown products glycerophosphocholine (GPC) and glycerophosphoethanolamine (GPE) [50] , was observed consistently for all transgene tumors (transfected with both wild type as well as inactive forms of nm23-1 and -2) but not for MDA-MB-435-V control tumors or MDA-MB-231 tumors. Results for all the animals in the study are summarized in Table 1. The ratio of PDE/PME was significantly higher for the transgene tumors compared to control tumors. A subset of spectra obtained for larger tumor volume sizes for the MDA-MB-435-1Tβ line showed similar differences in PDE/PME as the smaller volume sizes.

Observations made *in vivo* were also apparent in the spectra of cell extracts suggesting that differences in the GPC and GPE peaks for the transgene tumors are due to intrinsic cellular properties arising from transfection of cells with nm23 rather than due to *in vivo* physiological effects related to tumor vascularization or the fraction of necrosis.

Significant differences in intracellular and extracellular pH were also detected for the transgene tumors. Intracellular pH (pHi) was significantly lower for nm23-1 and nm23-2 transfected tumors compared to those derived from cells transfected with vector only (Table 1). Extracellular pH (pHe) was significantly higher for nm23-1, nm23-2 and nm23-2T transgene tumors compared to control tumors derived from cells with the vector only (Table 1). However, no significant differences in NTP/Pi or growth rate were detected for the different lines.
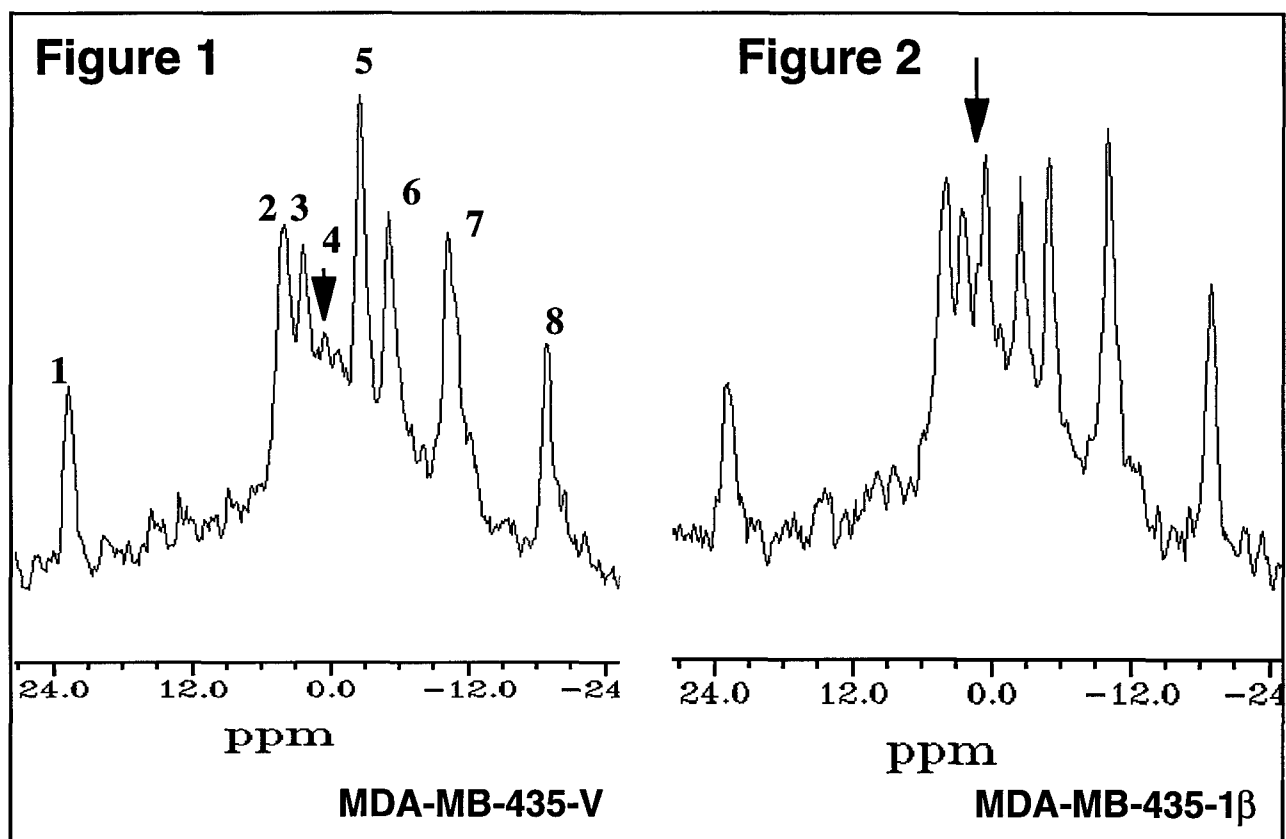
Figure 1 Fully relaxed ^{31}P NMR spectra obtained from an MDA-MB-435-V tumor. Peak assignments are (1) 3-APP (2) phosphomonoester (PME) (3) Inorganic phosphate (Pi) (4) phosphodiester (PDE) (5) phosphocreatine (PCr) (6) γ-NTP (7) α-NTP (8) β-NTP. **Figure 2**: Fully relaxed ^{31}P NMR spectra obtained from an MDA-MB-435-1β tumor. Peak assignments are as for Figure 1. Spectral acquisition parameters for *in vivo* tumors are detailed in Methods.

21

Table 1: Parameters obtained for *in vivo* tumors derived from the different cell lines are summarized in Table 1. Values represent Mean $\pm$ 1 S.E.M. n represents number of tumors studied *in vivo* for each group.

Tumor type	Tumor volume (mm^3)	PDE/PME = [GPE+GPC]/[PE+PC]	pHi	pHe	NTP/Pi
Control MDA-MB-435-V n=7	324 $\pm$ 42	0.60 $\pm$ 0.05	7.37 $\pm$ 0.07	6.8 $\pm$ 0.11	0.94 $\pm$ 0.05
Transgene MDA-MB-435-1β n=6	311 $\pm$ 45	1.45 $\pm$ 0.24[a]	7.16 $\pm$ 0.05[b]	7.17 $\pm$ 0.1[c]	0.8 $\pm$ 0.03
Transgene MDA-MB-435-1Tβ n=8	794 $\pm$ 74 (n=4) 296 $\pm$ 34 (n=4)	1.47 $\pm$ 0.13[a] 1.36 $\pm$ 0.09[a]	7.25 $\pm$ 0.08 7.37 $\pm$ 0.16	7.0 $\pm$ 0.14 7.08 $\pm$ 0.03	1.23 $\pm$ 0.07 0.83 $\pm$ 0.10
Transgene MDA-MB-435-2β n=6	255 + 19	1.36 $\pm$ 0.14[a]	7.15 $\pm$ 0.06[b]	7.09 $\pm$ 0.08[c]	0.90 $\pm$ 0.09
Transgene MDA-MB-435-2Tβ n=4	328 $\pm$ 58	1.34 $\pm$ 0.18[a]	7.19 $\pm$ 0.06	7.17 $\pm$ 0.22[c,d]	0.87 $\pm$ 0.07
Control MDA-MB-231 n=6	390 $\pm$ 45	0.71 $\pm$ 0.07	7.25 $\pm$ 0.04	7.0 $\pm$ 0.11	0.65 $\pm$ 0.08

[a]PDE/PME values significantly different from control MDA-MB-435-V tumors. P<0.005 (unpaired t-test), 99% confidence limit for Fisher Protected Least Significant Difference (Fisher PLSD) test (ANOVA).

[b]pHi values significantly different from control MDA-MB-435-V tumors. P<0.05 (unpaired t-test), 95% confidence limit for Fisher PLSD test (ANOVA).

[c]pHe values significantly different from control MDA-MB-435-V tumors. P<0.06 (unpaired t-test), 95% confidence limit for Fisher PLSD test (ANOVA); [d] 92% confidence limit.

DISCUSSION AND CONCLUSIONS

^{31}P NMR spectra of primary tumors in SCID mice revealed a dramatic and consistent difference in the phospholipid composition of control and transgene tumors formed by derivatives of MDA-MB-435 human breast carcinoma cells transfected with nm23 constructs. Since transgene tumors were formed by pooled transfected cells, these alterations cannot be due to peculiar properties of

Proprietary data

individual clone(s). Transgene tumors *in vivo* and cells in tissue culture exhibited a significantly higher amount of GPE and GPC relative to PE and PC levels when compared with control tumors *in vivo* and cells in tissue culture. Increased GPC and GPE levels were due to transfection of cells with nm23 and appeared to be unrelated to tumor vascularization or the necrotic fraction. Since the subset of 'large' MDA-MB-435-1Tβ tumors showed the same trends as the 'small' MDA-MB-435-1Tβ tumors, the increased GPC and GPE levels also appeared to be independent of tumor size. Differences in phospholipid compounds were detected for tumors transfected with both wild type and catalytically inactive forms of nm23-1 and nm23-2. Recent observations provide evidence both for and against the role of NDPK activity of nm23 in suppressing metastasis [51] [37, 52]; in our study the higher GPC, GPE levels for the transgene tumors appear to be independent of NDPK activity. Degradation of membrane phospholipids occurs through phospholipases A1 and A2 to GPC and GPE and then by GPC and GPE phosphodiesterases to choline and ethanolamine [53, 54]. The nm23 proteins may act by blocking GPC and GPE phosphodiesterase activity or upregulating phospholipase A1/A2 activity. Thus it will be interesting to determine effects of GPC and GPE phosphodiesterase inhibition or phospholipase A1/A2 upregulation on the invasive and metastatic behavior of the control cell line. Alternately, the differences in phospholipid degradation products may reflect differences in membrane turnover and degradation rates, and fatty acid requirements between the control and transfected cell lines. Cell lines with catalytically inactive NDPK appeared to deplete choline in the medium faster than the other cell lines since feeding these cells with fresh medium increased levels of PC. This may reflect differences in PC requirements for these cell lines.

^{31}P NMR spectroscopy revealed lower steady state intracellular pH (pHi) values for transgene tumors formed by MDA-MB-435-1β and MDA-MB-435-2β cells, as compared to control tumors. In contrast, this effect was not observed in tumors formed by MDA-MB-435-1Tβ and MDA-MB-435-2Tβ cells transfected with catalytically inactive nm23-1T and nm23-2T. Previous studies have shown that lowered pHi can inhibit GPC/GPE phosphodiesterase activity [55]. However such an inhibition does not appear to be a likely explanation for the elevated PDE levels in the transgene tumors observed here, since both MDA-MB-435-1Tβ and MDA-MB-435-2Tβ tumors exhibited high PDE/PME levels despite having pHi values very similar to control tumors. ^{31}P NMR spectroscopy revealed significantly higher extracellular pH (pHe) values for transgene tumors formed by MDA-MB-435-1β, MDA-MB-435-2β and MDA-MB-435-2Tβ cells. These results are particularly interesting, since only control cells, and MDA-MB-435-1Tβ cells retain high metastatic potential in a nude mice assay, while other transfected cell lines display a significantly decreased metastatic potential. Low extracellular pH can enhance the invasive behavior of human breast carcinoma cells. An acidic pericellular pH was found to increase the secretion of the active form of the lysosomal protease cathepsin B over time for human breast cancer cells [16]. The differences in intra- and extracellular pH between control and transgene tumors may be related to a higher build up of protons in the extracellular environment of more metastatic breast tumor cells, due to more efficient mechanisms for the extrusion of intracellular protons. If confirmed, these results may open new opportunities for diagnosis/prognosis of metastatic dissemination as well as potential targeting of pH regulation for anti-metastatic therapeutics.

This is the first *in vivo* observation which links activity of a putative metastasis suppressor nm23 gene to metabolic processes. Our data demonstrate the power of *in vivo* NMR in unraveling mechanisms controlling metastatic dissemination of tumor cells. These results also demonstrate the potential of noninvasive NMR to detect forms of gene therapy for suppression of metastasis which may involve transfection of cells with nm23.

Proprietary data

REFERENCES

1. Folkman, J., Watson, K., Ingber, D. and Hanahan, D., Induction of angiogenesis during the transition from hyperplasia to neoplasia. Nature *339*: 58-61, 1989.

2. Liotta, L.A., Steeg, P.S., Stetler-Stevenson, W.G., Cancer metastases and angiogenesis: an imbalance of positive and negative regulation. Cell *64*: 327-336, 1991.

3. Liotta, L., J. Kleinerman, and G. Saidel, Quantitative relationships of intravascular tumor cells, tumor vessels and pulmonary metastases following tumor implantation. Cancer Research *34*: 997-1004, 1974.

4. Folkman, J., The vascularization of tumors. Scientific American *234*: 59-73, 1976.

5. Folkman, J., How is blood vessel growth regulated in normal and neoplastic tissue ? Cancer Research *46*: 467-473, 1986.

6. Moses, M.A., The role of vascularization in tumor metastasis, *in* "Microcirculation in cancer metastasis", F. William Orr Buchanan, M.R., Weiss, L., Eds. 1991, CRC Press: p. 257-276.

7. Weidner, N., Semple, J.P., Welch, W.R. and Folkman, J., Tumor angiogenesis and metastasis - correlation in invasive breast carcinoma. New England Journal of Medicine *324*: 1-8, 1991.

8. Horak, E.R., Leek, R., Klenk, N., LeJeune, S., Smith, K., Stuart, N., Greenal, M., Stepniewska, K. and Harris, A.L. ., Angiogenesis, assessed by platelet/endothelial cell adhesion molecule antibodies, as indicator of node metastases and survival in breast cancer. Lancet *340*: 1120-1124, 1992.

9. Mareel, M.M., Baetselier, P., van Roy, F.M., Mechanisms of Invasion and Metastasis. 1991, CRC Press.

10. Shweiki, D., Itin, A., Soffer, D. and Kesbet, E., Vascular endothelial growth factor induced by hypoxia may mediate hypoxia-initiated angiogenesis. Nature *359*: 843-845, 1992.

11. Plate, K.H., Breier, Weich, H. and Risau, W., Vascular endothelial growth factor is a potential tumor angiogenesis facotr in human gliomas in vivo. Nature *359*: 845-848, 1992.

12. Cooper, R.G., Taylor, C.M., Choo, J.J. and Weiss, J.B., Elevated endothelial-cell stimulating angiogenic factor activity in rodent glycolytic skeletal muscles. Clinical Science *81*: 267-270, 1991.

13. Knighton, D.R., Hunt, T.K., Scheuenstuhl, H. and Banda, M., Oxygen tension regulates the expression of angiogenesis factor by macrophages. Science *221*: 1283-1285, 1983.

14. Knighton, D., Schumerth, S., and Fiegel, V., Environmental regulation of macrophage angiogenesis., *in* "Current Communications in Molecular Biology, Angiogenesis: Mechanisms in Pathobiology.", D.B. Rifkin Klagsbrun, M., Eds. 1987, Cold Spring Harbor Laboratory: p. 150-157.

15. Jensen, A.J., Hunt, B., Scheuenstuhl, B. and Banda, M.J., Effect of lactate, pyruvate and pH on secretion of angiogenesis and mitogenesis factors by macrophages. Laboratory Investigations *56*: 574-578, 1986.

16. Rozhin, J., Sameni, M., Ziegler, G. and Sloane, B.F., Pericellular pH affects distribution and secretion of Cathepsin B in Malignant cells. Cancer Research *54*: 6517-6525, 1994.

17. Kato, Y., Nakayama, Y., Umeda, M. and Miyazaka, K., Induction of 103kDa gelatinase/type IV collagenase by acidic culture conditions in mouse metastatic melanoma cell lines. J. Biol. Chem. *267*: 11424-11430, 1992.

18. Zhang, R.D., Fidler, I.J. and Price, J.E., Relative malignant potential of human breast carcinoma cell lines established from pleural effusions and a brain metastasis. Invasion and Metastasis *11*: 204-215, 1991.

19. Twentyman, P.R., Brown, J.M., Gray, J.W., Franko, A.J., Scoles, M.A., Kallman, R.F., A new mouse tumor system (RIF-1) for comparison of endpoint studies. J. Natl. Cancer Inst. *49*: 735-749, 1980.

20. Fidler, I.J., Orthotopic implantation of human colon carcinomas into nude mice provides a valuable model for the biology and therapy of metastasis. Cancer Metas. Review *10*: 229-243, 1991.

21. Ogan, M.D., Schmiedl, U., Mosley, M.E., Grodd, W., Paajanen, H., Brasch, R.C., Albumin labeled with Gd-DTPA; an intravascular contrast enhancing agent for magnetic resonance blood pool imaging: preparation and characterization. Invest. Radiol. *22*: 665-671, 1987.

22. Braunschweiger, P., Schiffer, L.M., Effect of dexamethasone on vascular function in RIF-1 tumors. Cancer Research *46*: 3299-3303, 1986.

23. Braunschweiger, P., Effect of cyclophosphamide on the pathophysiology of RIF-1 solid tumors. Cancer Research *48*: 4206-4210, 1988.

24. Takahashi, Y., Kitadai, Y., Bucana, C.D., Cleary, K.R. and Ellis, L.M., Expression of vascular endothelial growth factor and its receptor, KDR, correlates with vascularity, metastasis, and proliferation of human colon cancer. Cancer Research *55*: 3964-3968, 1995.

25. Jain, R.K., Transport of molecules across tumor vasculature. Cancer and Mestastasis Reviews *6*: 559-593, 1987.

26. Kuwatsuru, R., Shames, D., Muhler, A., Mintorovitch, J., Vexler, V., Mann, J.S., Cohn, F., Price, D., Huberty, J., Brasch, R.C., Quantification of tissue plasma volume in the rat by contrast-enhanced magnetic resonance imaging. Magnetic Resonance in Medicine *30*: 76-81, 1993.

27. Donahue, K., Burstein, D., Manning, W.J. and Gray, M.L., Studies of Gd-DTPA relaxivity and proton exchange rates in tissue. Magnetic Resonance in Medicine *32*: 66-76, 1994.

28. Schwickert, H.C., Roberts, T.P.L., Shames, D.M., van Dijke, C.F., Disston, A., Muhler, A., Mann, J.S. and Brasch, R.C., Quantification of Liver Blood Volume: Comparison of Ultra Short T1 Inversion Recovery Echo Planar Imaging (ULSTIR-EPI), with Dynamic 3D-Gradient Recalled Echo Imaging. Magnetic Resonance in Medicine *34*: 845-852, 1995.

29. Rubin, P., Casarett, G., Microcirculation of tumors part I: Anatomy, function, and necrosis. Clinical Radiology *17*: 220-229, 1966.

30. Dvorak, H.F., Nagy, J.A., Dvorak, J.T. and Dvorak, A.M., Identification and characterization of the blood vessels of solid tumors that are leaky to circulating macromolecules. American Journal of Pathology *133* : 95-109, 1988.

31. Demsar, F., Roberts, T.P.L., Schwickert, H.C., Shames, D.M., van Dijke, C.F., Mann, J.S., Saeed M., Brasch, R.C., A MRI spatial mapping technique for microvascular permeability and tissue blood volume based on macromolecular contrast agent distribution. Magnetic Resonance in Medicin *37* : 236-242, 1997.

32. Reeve, J.G., Twentyman, P.R., Ploidy distribution of tumor cells derived from induced and spontaneously arising metastases of a murine radiation-induced sarcoma, RIF-1. Brit. J. Cancer Clin. Oncol. *18* : 1001-1006, 1982.

33. Steel, G.G., Growth kinetics of tumours: Cell population kinetics in relation to the growth and treatment of cancer. 1977, Oxford: Clarendon Press.

34. Hirst, D.G., Denekamp, J., Hobson, B., Proliferation kinetics of endothelial and tumour cells in three mouse mammary carcinomas. Cell Tissue Kinetics *15* : 251-261, 1982.

35. Aznavoorian, S., Murphy A. N., Stetler-Stevenson, W. G., Liotta, L. A., Molecular aspects of tumor cell invasion and metastasis. Cancer *71* : 1368-1383, 1993.

36. Steeg, P.S., Bevilaqua, G., Kopper, L., Thorgeirsson, U.P., Talmadge, J.E., Liotta, L.A., Sobel, M.E., Evidence for a novel gene associated with low tumor metastatic potential. J. Natl. Cancer Inst. *80* : 200-204, 1988.

37. De La Rosa, A., Williams, R.L., Steeg, P.S., Nm23/nucleoside diphosphate kinase: Toward a structural and biochemical understanding of its biological functions. Bioessays *17* : 53-62, 1995.

38. MacDonald, N.J., De La Rosa, A., Steeg, P.S., The Potential role of *nm23* in Cancer Metastasis and cellular differentiation. European Journal of Cancer *31A* : 1096-1100, 1995.

39. Urano, T., Takamiya, K., Furukawa, K. and Shiku, H., Molecular cloning and functional expression of the second mouse nm23/NDP kinase gene, nm23-M2. FEBS Lett. *309* : 358-362, 1992.

40. Rosengard, A.M., Krutrzsch, H.C., Shearn, A., Biggs, J.R., Barker, E., Margulies, I.M.K., King, C.R., Liotta, L.A. and Steeg, P.S., Reduced NM23/Awd protein in tumor metastasis and aberrant Drosophilia development. Nature *342* : 177-180, 1989.

41. Stahl, J.A., Leone, A., Rosengard, A.M., Porter, L., King, C.R., Steeg, P.S., Identification of a second human nm23 gene, nm23-H2. Cancer Res. *51* : 445-449, 1991.

42. Ishikawa, N., Shimada, N., Munakaata, Y., Watanabe, K., Kimura, N., Isolation and characterization of a gene encoding rat nucleoside diphosphate kinase. J. Biol. Chem. *267* : 14366-14372, 1992.

43. Shimada, N., Ishikawa, N., Munakata, Y., Toda, T., Watanabe, K., Kimura, N., A second form (b isoform) of nucleoside diphosphate kinase from rat. J. Biol. Chem. *268* : 2583-2589, 1993.

44. Kelsell, D., Black, D., Solomon, E., Spur, N.K., Localization of a second nm23 gne, NME2, to chromosome 17q21-22. Genomics *17* : 522-524, 1993.

45.   Backer, J.M., Mendola, C.E., Kovesdi, I., Fairhurst, J.L., O'Hara, B., Shows, T.B., Mathews, S., Murty, V.V.S., Chaganti, R.S.K., Chromosomal localization and nucleoside diphosphate kinase activity of human metastasis- suppressor NM23-1 and NM23-2. Oncogene *8* : 497-502, 1993.

46.   Backer, J.M., Mendola, C.E., Price, J., Thomson, J., Sperry, R.G., Oiseth, S., Hamby, C.V. NME2 (nm23-2) gene may control the expression of metastatic phenotype. in *88th Annual Meeting of American Association for Cancer Research*. 1996. Washington, D.C.:

47.   Gilles, A.M., Presecan, E., Vonica, A., Lascu, I., Nucleoside diphosphate kinase from human erythrocytes. Structural characterization of the two polypeptide chains responsible for heterogeneity of the hexameric enzyme. J. Biol. Chem. *266* : 8784-8789, 1991.

48.   Gillies, R., Liu, Z., Bhujwalla, Z.M., 31P MRS measurements of extracellular pH of tumors using 3-aminopropylphosphonate. Am. J. Physiol. *267* : C195-C203, 1994.

49.   Moon, R.B. and J.H. Richards, Determination of intracellular pH by 31P magnetic resonance. J. Biol. Chem. *248* : 7276-7278, 1973.

50.   Evanochko, W.T., Sakkai, T.T., Ng, T.C., Krishna, N.R., Kim, H.D., Zeidler, R.B.,Ghanta, V.K., Brockman, R.W., Schiffer, L.M., Braunschweiger, P.G., Glickson, J.D., NMR study of in vivo RIF-1 tumors: Analysis of perchloric acid extracts and identification of 1H, 31P and 13C resonances. Biochim. Biophys. Acta *805* : 104-116, 1984.

51.   Russell, R.L., Geisinger, K.R., Mehta, R.R., White, W.L., Shelton, B., Kute, T.K., nm23-Relationship to the Metastatic Potential of Breast Carcinoma Cell Lines, Primary Human Xenografts, and Lymph Node Negative Breast Carcinoma Patients. Cancer *79* : 1158-65, 1997.

52.   Easty, D.J., Maung, K., Lascu, I., Veron, M., Fallowfield, M.E., Hart, I.R. and Bennett, D.C., Expression of NM23 in human melanoma progression and metastasis. Brit. J. Cancer *74* : 109-114, 1996.

53.   Daly, P.F., Lyon, R.C., Faustino, P.J., Cohen, J.S., Phospholipid Metabolism in cancer cells monitored by 31P NMR Spectroscopy. J. Biol. Chem. *262* : 14875-14878, 1987.

54.   Daly, P.F., Zugmaier, G., Sandler, D., Carpen, M., Myers, C.E. and Cohen, J.S., Regulation of the cytidine phospholipid pathways in human cancer cells and effects of 1-beta-D-arabinofuranosylcytosine: a noninvasive 31P nuclear magnetic resonance study. Cancer Research *50* : 552-7, 1990.

55.   Galons, J.P., Job, C., Gillies, R. J., Increase of GPC levels in cultured mammalian cells during acidosis: A 31P MR spectroscopic study using a continous bioreactor system. Mag. Res. Med. *33* : 422-6, 1995.

MCMR-RMI-S   (70-1y)   21 Feb 03

MEMORANDUM FOR Administrator, Defense Technical Information
Center (DTIC-OCA), 8725 John J. Kingman Road, Fort Belvoir,
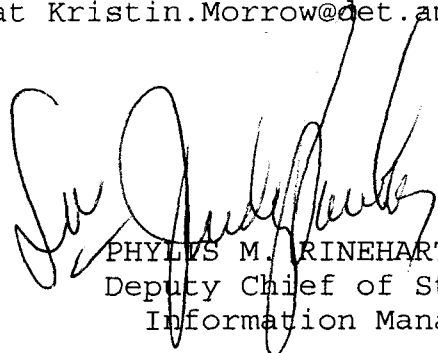VA   22060-6218

SUBJECT: Request Change in Distribution Statement

1. The U.S. Army Medical Research and Materiel Command has
reexamined the need for the limitation assigned to technical
reports written for this Command. Request the limited
distribution statement for the enclosed accession numbers be
changed to "Approved for public release; distribution unlimited."
These reports should be released to the National Technical
Information Service.

2. Point of contact for this request is Ms. Kristin Morrow at
DSN 343-7327 or by e-mail at Kristin.Morrow@det.amedd.army.mil.

FOR THE COMMANDER:

Encl

PHYLIS M. RINEHART
Deputy Chief of Staff for
Information Management

ADB263458   ADB282838
ADB282174   ADB233092
ADB270704   ADB263929
ADB282196   ADB282182
ADB264903   ADB257136
ADB268484   ADB282227
ADB282253   ADB282177
ADB282115   ADB263548
ADB263413   ADB246535
ADB269109   ADB282826
ADB282106   ADB282127
ADB262514   ADB271165
ADB282264   ADB282112
ADB256789   ADB255775
ADB251569   ADB265599
ADB258878   ADB282098
ADB282275   ADB232738
ADB270822   ADB243196
ADB282207   ADB257445
ADB257105   ADB267547
ADB281673   ADB277556
ADB254429   ADB239320
ADB282110   ADB253648
ADB262549   ADB282171
ADB268358   ADB233883
ADB257359   ADB257696
ADB265810   ADB232089
ADB282111   ADB240398
ADB273020   ADB261087
ADB282185   ADB249593
ADB266340   ADB264542
ADB262490   ADB282216
ADB266385   ADB261617
ADB282181   ADB269116
ADB262451
ADB266306
ADB260298
ADB269253
ADB282119
ADB261755
ADB257398
ADB267683
ADB282231
ADB234475
ADB247704
ADB258112
ADB267627